ADVANCED FUNCTIONAL MATERIALS
www.afm-journal.de

Bilayer Solar Crystallizer by a Directional Liquid Transport Fabric for Stable Brine Treatment and Ion Recycling

Zhang Hanchao, Yang Qiang, Wu Yudong, Meng Jie, Guan Xiaoyang, Jiang Yi, Chen Jinxing, and Fan Jintu**

Directional and asymmetric liquid transport (DALT) materials are promising for human moisture management and atmospheric water harvesting, but they are less known for their benefits in brine transportation and salt crystallization. Here, it is discovered a unique salt crystallization behavior of the DALT fabric which the salt with porous structure prefers to crystallize on the surface rather than in the inner space of the DALT fabric. Based on that, a bilayer solar crystallizer has been engineered by integrating this DALT fabric as an external crystalline interface with an inner adsorbent loaded wicking layer for simultaneous brine treatment and resource recovery. This bilayer structure separated the brine wicking channel from the crystallization interface, thereby reducing the efficiency losses by salt scaling to maintain the stable evaporation rate (>1.6 L/m^2/h) during the brine treatment. Furthermore, the adsorbent in the inner layer ($Li_4Ti_5O_{12}$ (LTO)) can recover Li^+ by the adsorption (alkaline)-desorption (acid) cycle, and the successful LiCl recovery from the brine with high efficiency (>81%) and purity (94.8%) is demonstrated by this bilayer solar crystallizer. This work fills in the understanding of brine transportation and salt crystallization in DALT materials, demonstrating the great potential for its application in wastewater treatment and resource recovery.

1. Introduction

While industrialization significantly promoted socioeconomic development,[1,2] the generation of hypersaline brine by-products during industrial processes (e.g., petrochemical manufacturing, textile dyeing, and seawater desalination) imposes substantial environmental constraints. These brine by-products require prohibitive energy expenditures and capital investments for treatment due to their elevated salinity.[3,4] Meanwhile, it concurrently serves as the reservoir of high-value components[5](e.g., metal ions, organic dyes, and polymer monomers) with significant economic potential for recovery.[6,7] Consequently, developing integrated technologies for efficient brine treatment coupled with selective resource recovery represents a critical technological challenge with both immediate and long-term implications.

Solar-driven crystallizers,[8,9] which harvest solar energy to generate localized heat for interfacial evaporation and salt crystallization, has emerged as a sustainable and cost-effective brine management strategy.[10] While conventional designs focus on freshwater production and salt harvesting, progressive salt deposition on photothermal interfaces inevitably obstructs light absorption and water transport,[11,12] leading to system failure. Although new designs of the three-dimensional (3D) crystallizer attempt to decouple light absorption and evaporation interface to mitigate salt shielding effects,[13,14] persistent scaling issues caused by the actual brine,[15] particularly scaling from the divalent cations (Mg^{2+}, Ca^{2+}) remain unresolved, severely limiting practical implementation.

Directional and asymmetric liquid transport (DALT),[16,17] a ubiquitous phenomenon observed in biological systems such as cactus spines and butterfly wings, has inspired the development of engineered materials capable of tunable liquid manipulation through wettability or structural gradients.[17,18] While the hydrodynamic principles governing DALT have been extensively characterized,[19] critical knowledge gaps persist regarding brine transport dynamics and crystallization behavior on gradient surfaces, particularly under hypersaline conditions. Notably, recent studies reveal that superhydrophobic-hydrophilic heterointerfaces can modulate salt crystallization patterns through interfacial tension engineering,[18,20] suggesting a novel pathway to control scaling phenomena in DALT-enabled systems. This

Z. Hanchao, Y. Qiang, W. Yudong, M. Jie, G. Xiaoyang, F. Jintu
School of Fashion and Textile
The Hong Kong Polytechnic University
Hung Hom, Kowloon, Hong Kong 999077, China
E-mail: hanchao.zhang@polyu.edu.hk; jin-tu.fan@polyu.edu.hk
Z. Hanchao, F. Jintu
Research Centre of Textiles for Future Fashion
The PolyU Academy for Interdisciplinary Research
Kowloon, Hong Kong 999077, China
Z. Hanchao, J. Yi
Department of Civil and Environmental Engineering
The Hong Kong Polytechnic University
Hung Hom Kowloon, Hong Kong 999077, China
Z. Hanchao, F. Jintu
PolyU Xingguo Technology and Innovation Research Institute
The Hong Kong Polytechnic University
Kowloon, Hong Kong 999077, China
C. Jinxing
Institute of Functional Nano and Soft Materials (FUNSOM)
Jiangsu Key Laboratory of Advanced Negative Carbon Technologies
Soochow University
199 Ren'ai Road, Suzhou, Jiangsu 215123, China

DOI: 10.1002/adfm.202511412

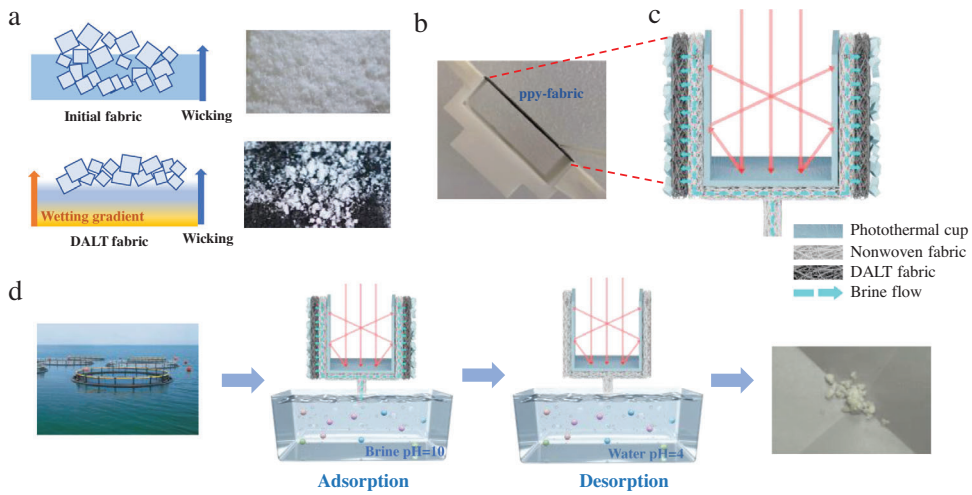

Figure 1. The schematic diagram and images of the salt crystallization on the initial fabric and DALT fabric a); The optical photograph of the DALT fabric b); and it applies to the bilayer structured solar crystallizer c); The flow diagram for the Li^+ recovery during the brine treatment d).

mechanistic insight motivates our hypothesis that DALT materials will fundamentally alter brine transport-crystallization coupling compared to conventional wicking substrates, potentially revolutionizing fouling mitigation strategies in solar crystallizers.

In this work, through a systematic investigation of brine transport and crystallization kinetics on porous DALT fabrics, we discovered a unique surface crystallization phenomenon. Contrary to conventional fabrics, where salt precipitates within internal pores and simultaneously on surfaces, the salt with a loose structure is preferred to be crystallized on the surface of DALT fabrics due to the continuous brine flow (**Figure 1a**). Combining in situ microscopy, X-ray diffraction analysis, and computational fluid dynamics simulations, we elucidated the governing mechanism: the wettability gradient generated in the thickness of the DALT fabric will suppress the nucleation of salt in the inner of the fabric while promoting surface-directed crystal growth. Building upon this discovery, we engineered a bilayer 3D crystallizer architecture (Figure 1b) by integrating DALT fabric as an external crystalline interface with an inner adsorbent-loaded wicking layer. This bilayer-structured design separated the brine wicking channel from the crystallization interface, thereby reducing the salt scaling-induced efficiency losses to maintain the stable evaporation rate (>1.6 $L/m^2/h$) for the entire brine treatment. Furthermore, the adsorbent in the inner layer can absorb valuable ions during the brine evaporation, and the ions adsorption efficiency in this solar crystallizer is significantly enhanced compared to the bulk solution adsorption due to the increase in target ions concentration with the water evaporation and the sufficient contact with the adsorbent. Benefiting from that, the successful Li recovery from the seawater and brine with high efficiency and purity was demonstrated by integrating the Li adsorbent ($Li_4Ti_5O_{12}$) into this bilayer solar crystallizer (Figure 1c). The findings of this work provide an insightful understanding of brine transportation and salt crystallization in DALT materials and further promote its application for brine transportation, desalination, salt crystallization, solar evaporation, and resource recovery fields.

2. Results

2.1. Crystallization Behavior of DALT Fabric

In our previous work,[21] we developed a DALT fabric, polypyrrole modified fabric (ppy-fabric), by the interfacial polymerization methods (Figure S1, Text S1). Briefly, the pyrrole was selectively polymerized on the one side of the nonwoven fabric surface to generate *Turing* patterns. The roughness of the fiber surface was increased by the nanostructure of the *Turing* pattern, which modified one side of the ppy-fabric from super-hydrophilic to a superspreading surface. This design developed the wetting gradient between the double side of the ppy-fabric, and the liquid can be transported from the super-hydrophilic (Figure S1a) to the superspreading surface at an ultrafast rate (Figure S1b). Thus, the initial fabric shows the same wetting area between the double sides (Figure S1c), but the ppy-fabric shows a great difference in wetting area between the double sides (Figure S1d). However, the wetting gradient and the superhydrophilic surface (Figure S2) will greatly influence the brine transportation and the salt crystallization process. To investigate that, the crystallization experiment of the nonwoven fabric and the ppy-fabric was tested in the vertical wicking and evaporation device with 2 mol L^{-1} NaCl solution (**Figure 2a**). It can be observed that the loose NaCl was crystallized on the single surface of the ppy-fabric, while less NaCl salt was observed on the front surface of the initial fabric (Figure 2b). The evaporation rate of the ppy-fabric (0.130 L/m^2 h) is slightly higher than that of the initial fabric (0.113 L/m^2 h) (Figure S3), which means the salt crystallization rate is similar in these two fabrics at the same time. To further study, the salt on the front surface of the fabric was collected and weighed (Figure 2c), and more than 81% of the salt crystal was collected on the front surface of the ppy-fabric but only 53% of the salt crystal was collected on the front surface of the initial fabric, and the residual salt is on the back surface or the interspace of the fabric (Figure 2c). This conclusion was further proved by the optical microscope examination, which showed that many salt crystals were observed in the interspace of the initial fabric (Figure 2d–g), but the salt

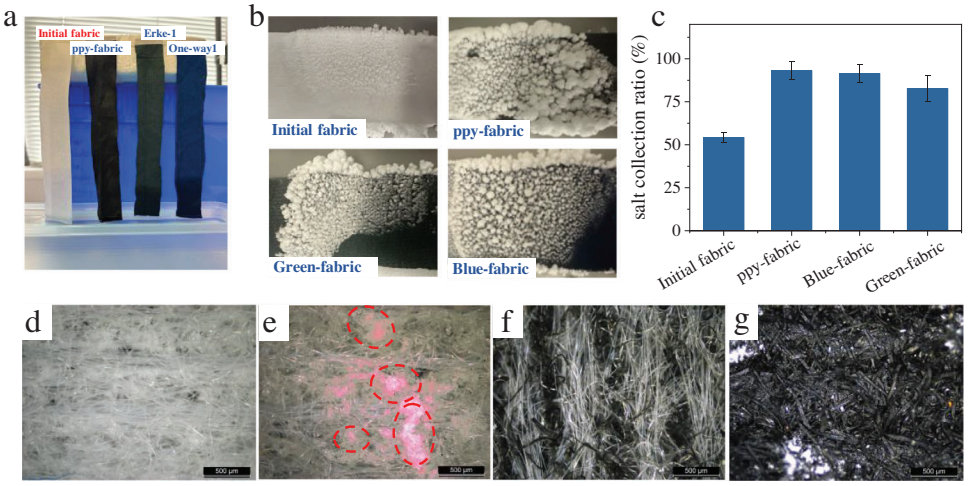

Figure 2. The vertical crystallization experiment a), the picture of the salt on the front surface b), and the weight ratio of the salt collected from different fabrics c). The optical microscope of the initial fabric before d) and after e) salt crystallization. The optical microscope of the ppy-fabric before f) and after g) salt crystallization. The red cycle in e is the NaCl salt in the inner space of the fabric.

crystals are mostly on the fiber surface of the ppy-fabric. Therefore, the difference in salt crystallization behavior between these two fabrics is because the salt only crystallized on the surface of the ppy-fabric, while it was crystallized on the double sides and the interspace of the initial fabric. Moreover, this phenomenon is also related to salt concentration (Figure S4), and the salt is more likely to crystallize in the inner space of the fabric under high concentration, but most salt can still be collected (>80%) from the front surface of the ppy-fabric at different salt concentrations.

Moreover, the salt crystal on the ppy-fabric is more porous than that of the initial fabric, which also led to a greater number of salt crystals visually. The X-ray diffraction (XRD) patterns (Figure S5) of the salt collected from the initial fabric and ppy-fabric show the same peak locations of the face-centered cubic (FCC) NaCl crystals, indicating that the crystalline phase of the NaCl has not changed in the DALT fabric. However, the specific surface area of the salt collected from the ppy-fabric surface is 2.13 times that of the initial fabric (Figure S6), demonstrating that the one-way brine transportation across the ppy-fabric reduces the size of crystal particles and increases the porosity of the salt.

Besides the ppy-fabric, other commercial DALT fabrics, green and blue-fabric, were also used for this vertical evaporation experiment and observed similar results (Figure 2b). The NaCl is preferred to crystallize on the surface of the commercial DALT fabric to generate loose crystals, and 78%-81% salt can be collected on the front surface of the DALT (Figure 2c). That means the one-way liquid transportation properties of the porous materials alter the brine transportation and the salt crystallization behaviors, and the crystallization location and morphology of the salt are greatly changed in the DALT fabric.

2.2. Mechanism of the Surface Crystallization of DALT Fabric

To further investigate the crystallization mechanism in the DALT fabric, a COMSOL simulation was conducted to investigate the brine transportation and crystallization process in the DALT fabric. In vertical evaporation, the brine is wicked by the fabric from the bulk solution to the top surface, and the water on the front surfaces of the fabric is evaporated under natural volatilization, driving the brine continually transported from the interspace to the front surface. With the brine evaporation, the salt ions on the front interface of the fabric will be increased to saturation and then crystallize. At this time, the salt concentration on the front surface is much higher than that in the interspace, and a concentration gradient will be developed to drive the salt ions back diffused to the interspace. The step function (φ, Equation. 1) was developed for the measurement of the crystallization degree of the NaCl

$$\varphi = step\ (c/cwt) \tag{1}$$

where the c and c_{wt} are the actual and saturation concentration, respectively. The $\varphi = 0$ means it has no crystallization, and the $\varphi = 1$ means the generation of the crystals.

For the initial fabric, the salt ion concentration will be increased on the front surface with the brine evaporation (**Figure** 3a,c,d). Meanwhile, the back diffusion of salt ions will increase the ion concentration from the surface to the interspace of the fabric, resulting in salt crystallization in the inner space of the fabric (Figure 3d). This result is consistent with the experimental phenomenon in the evaporation experiment. In contrast, the wetting gradient in the DALT will continually drive the liquid transported from the inner space on the front surface (Figure 3b), ensuring fast brine flow supplies to the front surface of the fabric. Thus, the ion concentration on the evaporation surface of the DALT fabric is lower than that of the initial fabric, and the ions, which are the main reason for the back diffusion of the salt ions on the DALT fabric, were lower than the initial fabric. Furthermore, the salt ion concentration in the inner space of the fabric will be decreased by this process (Figure 3b), which would suppress the nucleation process of salt ion crystallization. Benefiting from that, this one-way brine transportation promoted the salt to

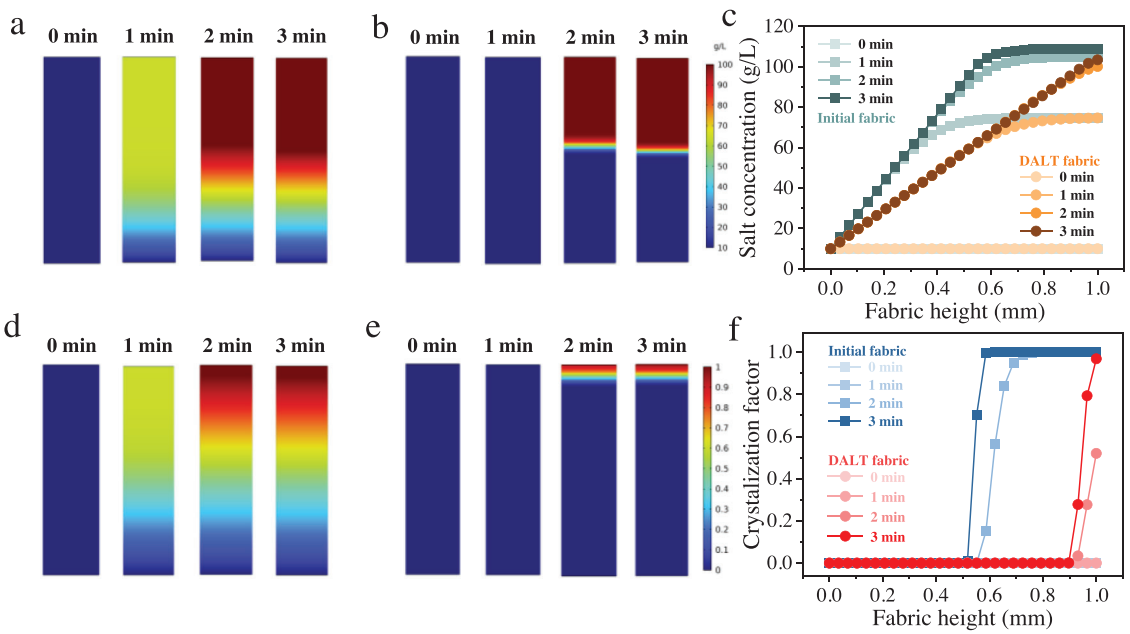

Figure 3. The theoretical simulation of the NaCl solution transportation along the fabric height in the initial fabric a) and the ppy-fabric b), and the salt concentration curve c). The theoretical simulation of the salt crystallization ratio along the fabric height in the initial fabric d), the ppy-fabric e), and the salt crystallization ratio curve f). The salt crystallization ratio is obtained from the Brinkman equation, and the 0 represents no salt crystallization, while the 1 represents complete crystallization. The NaCl concentration in the bulk solution is 2 mol L^{-1}.

crystallize on the front surface (Figure 3d) and minimized the scaling of the inner space.

Besides that, the continuous transport of the brine across the thickness of the DALT fabric will break the balance of the crystal solution. According to the crystallization theory,[22] the size of the NaCl crystal is controlled by the nucleation and growth processes, which are strongly related to the supersaturation degree of the brine. The higher supersaturation degree of the brine is beneficial to the crystal nucleation and growth, resulting in a larger size of the salt crystal. Meanwhile, the fast one-way transportation along the thickness of the ppy-fabric compresses the crystal growth space and shortens the crystal growth time (Figure 3d), thus it will have a small crystal size with a porous structure on the surface for the DALT fabric (Figure 3e,f).

2.3. Develop a Bilayer Solar-Based Crystallizer for Stable Brine Evaporation

Based on the above results, the salt will crystallize in the inner space of the initial fabric under high concentration, which will block the wicking channel to hinder the brine transportation. In contrast, the DALT fabric only crystallizes the salt on the surface, and it is beneficial for continual brine wicking and evaporation. Therefore, this unique brine transportation and salt crystallization behavior of DALT inspired us to apply it to the solar crystallizer for stable brine evaporation. In the traditional 3D-cup solar crystallizer, a single layer of the nonwoven fabric is wrapped around the solar-absorbed cup, and the heat from the photothermal conversion of the solar-absorbed cup can be transferred into the nonwoven fabric for the brine evaporation. This design separates the photothermal conversion interface (inner space of the cup) from the brine transportation channel (nonwoven fabric). Nevertheless, the accumulation of salt crystals in the interspace of the nonwoven fabric, especially under high salt concentration, will suspend the brine wicking and evaporation. This work uses the ppy-fabric to wrap around the non-woven fabric to develop the bilayer 3D solar crystallizer (Figures 1b and 4a), and the carbon black coated inside of a cup is used as the photothermal material. The ppy-fabric can rapidly transport the brine from the inner surface (non-woven fabric) to the outer surface for water evaporation, and the salt will crystallize on the outer surface of the ppy-fabric. This design separates the wicking channel for the brine (nonwoven fabric) from the crystallization surface (outer surface of the ppy-fabric), thus the salt accumulation has less influence on the brine evaporation efficiency in this bilayer system. Furthermore, such a bilayer design will also facilitate the extraction and recovery of the Li^+, which will be shown and discussed in the following part.

As shown in Figure 4b, the water evaporation rate of the single and bilayer solar evaporator is similar in the dark. However, under one sun irradiation, the evaporation rate of the bilayer solar crystallizer is 2.63 L m^{-2} h, which is 1.25 times that of the single-layer solar crystallizer. The main reason is that the outer surface of the ppy-fabric is black, and it will absorb the scattered light to further increase the evaporation efficiency. Furthermore, the outer surface temperature measured by the infrared camera shows that the temperature on the outer surface of the bilayer solar crystallizer is 0.2 to 1.3°C higher than that of the single-layer(Figure 4c), and the temperature difference is more obvious in the bottom of the solar crystallizer, indicating that the black ppy-fabric can absorb the scattering light for the photothermal conversion to enhance water evaporation rate. Since the bottom of the cup receives more reflected light, it also

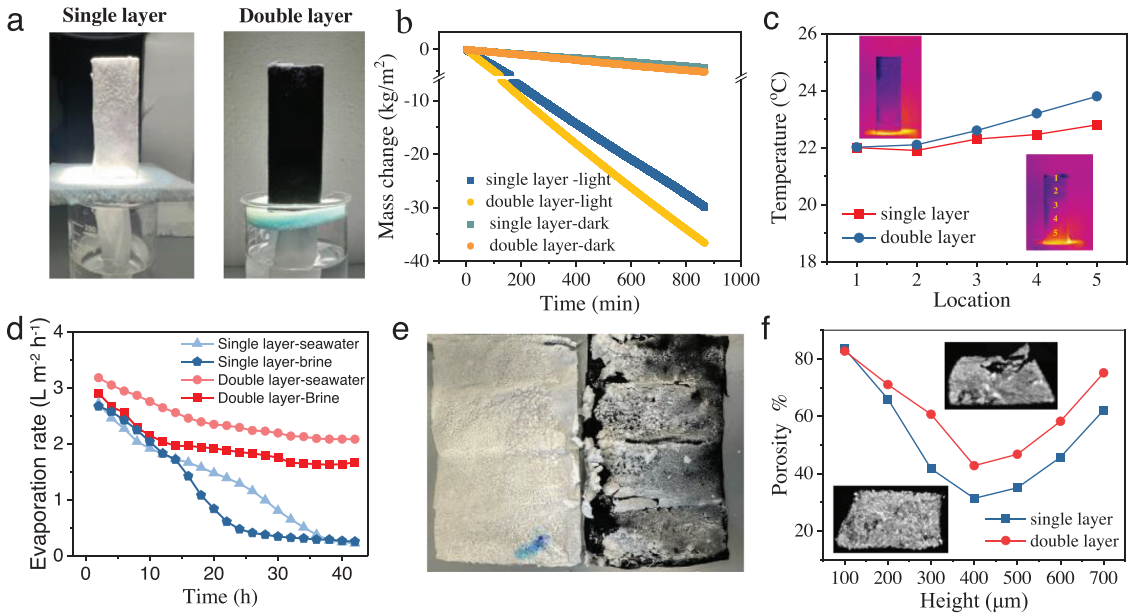

Figure 4. The device a), the evaporation rate b), and the surface temperature c) of the single-layer and bilayer solar-based crystallizer. The evaporation rate d) and the surface salt accumulation picture e) of the solar-based crystallizer for the seawater and brine evaporation. The surface salt accumulation picture (e) and the three-dimensional reconstruction by the solar-based crystallizer's micro-computerized tomography f) for the brine evaporation.

has a higher temperature from the photothermal conversion of ppy.

The initial seawater and the concentrated seawater (ion concentration shown in text S1) were used as the brine to test the long-term evaporation performance of the single-layer and the bilayer solar-based crystallizer. As shown in Figure 4d, the seawater evaporation rate of the single-layer solar crystallizer gradually reduces to less than 0.1 L m^{-2} h during the 40 h irradiation. Meanwhile, the available evaporation can only maintain 24 h for the high concentration brine by the single-layer structure solar crystallizer. In contrast, the bilayer solar crystallizer can achieve steady evaporation over 40 h in the seawater and brine, and the decrease of evaporation rate in the initial stage (10 h) is mainly due to the salt accumulation shielded the light absorption of the ppy-fabric. Meanwhile, it can be observed that the salt crystal in the bilayer structured solar crystalized looser than that on the single layer (Figure 4e), and it is probably the main reason for the stable brine wicking and evaporation in the bilayer solar crystallizer. Besides Na^+, the Ca^{2+} and Mg^{2+}, will generate the scaling to blockage the pores of the wicking channel, which is the main reason for the out of the work for the solar crystallizer in the actual brine. The bilayer structure with the ppy-fabric facilitated the salt to crystallize on the outer surface of the solar crystallizer, reducing the influence of the scaling on the brine wicking and evaporation. After the evaporation process, the salt on the outer layer of the solar crystallizer can be easily removed by the mechanical method,[15] and the detachable and replaceable ppy-fabric is convenient for the concentrative salt removal or collection treatment.

To accurately analyze the morphology of salt crystals on the fabric surface, micro-computerized tomography (CT)[22] was used to reconstruct salt crystals in three dimensions on the single-layer and bilayer solar crystallizer (Figure 4f). Based on the calculation of the three-dimensional model of salt crystals, the porosity of the fabric/salt compound is first decreased and then recovered along the thickness of the nonwoven fabric (single layer) and ppy fabric (double layer). The ppy-fabric has a similar porosity to the nonwoven fabric because the ppy film on the cellulose fiber has less change in its structure. However, the porosity of the first 400 μm single-layer structure is lower than that of the bilayer structure, mainly due to the higher salt concentration in the inner space of the nonwoven fabric. This result is consistent with the phenomenon in Figure 2 that the salt was crystallized in the inner space and surface of the nonwoven fabric, while it is preferred to crystallize on the surface of the ppy-fabric. Furthermore, the porosity of the bilayer structure is higher than that of the single-layer structure on the top 100 μm (Figure 4f), which is only from the porosity of the single salt, further demonstrating that the salt crystals on the ppy-fabric surface are looser than those of the non-woven fabric. Thus, due to the separation of the wicking channel from the crystallization interface and the porous salt crystals, the bilayer solar-based crystallizer shows more stable performance during the brine evaporation. Recent studies have designed a novel structure for the stable long-term evaporation of seawater or brine,[23–25] but the high solar absorption efficiency and the zero-liquid-discharge properties are still the advantages of this bilayer structure solar evaporator. Furthermore, this DALT fabric could also be applied to other solar evaporators as the wicking material to further enhance its evaporation stability.

2.4. Selective Ion Adsorption by the Bilayer Solar Crystallizer

The traditional solar crystallizer has poor selectivity for salt crystallization, and the collection of mixed salt has low value for further utilization.[26] Meanwhile, salt recovery is more challenging for ions with low concentrations in brine, although it has high

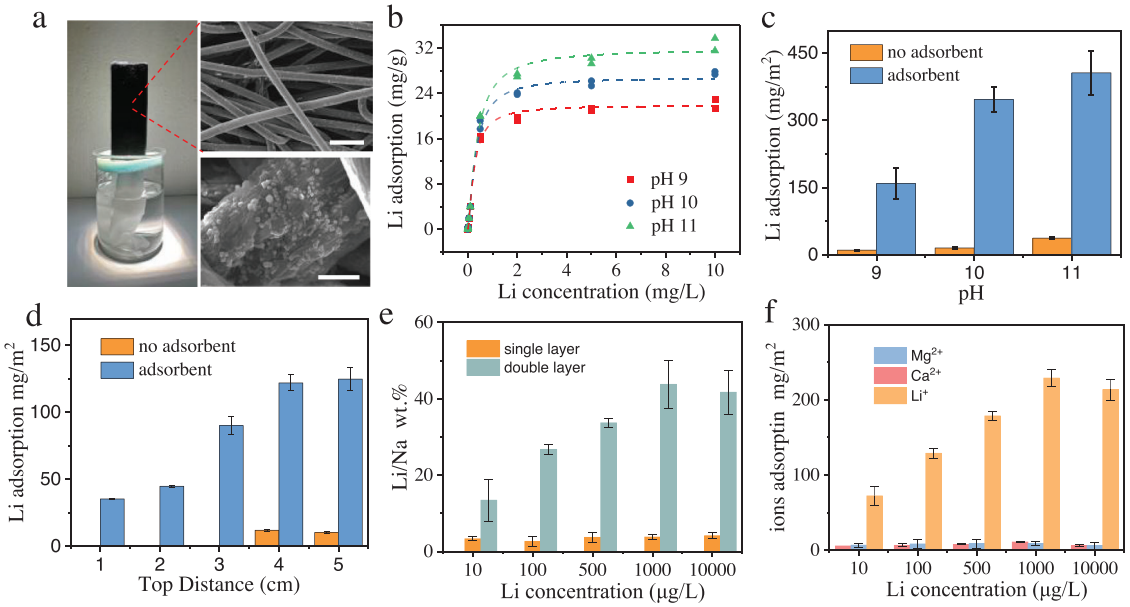

Figure 5. The picture of the bilayer solar-based crystallizer and the scanning electron microscope (SEM) picture of the fiber with Li adsorbent a); The Li adsorption kinetics of the LTO under different pH b); The Li adsorption kinetics of the LTO loaded ppy-fabric under different pH c); The Li^+ adsorption under different height of the bilayer solar-based crystallizer with and without adsorbent, Li concentration in bulk solution is 100 μg L^{-1} d); The Li/Na ratio of the single- and the inner layer of the bilayer solar crystallizer under different Li concentrations e). The ions' adsorption in the inner layer of the bilayer solar crystallizer under different Li concentrations f). The concentration of Na^+ in the bulk solution is 10 g L^{-1}.

economic value, such as Li^+, Au^+, Ag^+, etc. In this work, we integrated the lithium adsorbent, $Li_4Ti_5O_{12}$ (LTO), into this bi-layer solar crystallizer to extract lithium from seawater to proof-of-concept the low-concentration ions recovery by the bilayer solar-based crystallizer. Projections indicate an eightfold to tenfold increase in lithium demand from 2023 to 2050, reaching 1,607 kilotonnes, predominantly driven by the electric vehicles industry. Lithium extraction from low-quality brine sources is a promising path due to the huge reserves of lithium in brine and seawater. Li^+ can occupy the tetrahedral 8a sites of the LTO with a spinel structure,[27] and these sites will exchange the Li^+ cycle under alkaline and acidic conditions. After integrating the LTO into the fabric, the fabric can adsorb Li^+ under alkaline conditions (pH 9–11) and desorb the Li^+ under acid conditions (pH 3–5), thereby realizing the reversible absorption and desorption for lithium extraction.

As shown in **Figure** 5a, the LTO is loaded on the inner layer of nonwoven fabric by spraying coating (Figure S7), and the single layer of nonwoven fabric with and without the LTO is also used for the comparison. The scanning electron microscope (SEM) images show the LTO uniformly loaded on the fiber surface of the nonwoven fabric (Figure 5a). Furthermore, the adsorption capacity of the LTO-loaded fabric increased from 20.4 to 31.6 mg/g with the pH increase from 9 to 11 (Figure 5b), indicating that a higher pH is beneficial for Li adsorption. Meanwhile, the LTO-modified nonwoven fabric shows 153.6 to 436.5 mg m^{-2} adsorption capacity under pH 9 to 11 (Figure 5c), which is 32–48 times that of the nonwoven fabric without LTO.

In the bilayer solar crystallizer, the Li^+ adsorption shows a difference along the height, and more Li is absorbed by the bottom side due to the prioritized contact with the brine (Figure 5d). To study the Li adsorption performance under different types of brine, the mixed solution of LiCl and NaCl with gradient ratios of $10/10^7$, $100/10^7$, $500/10^7$, $1000/10^7$, and $10000/10^7$ were used for the simulation of the brine with a low concentration of Li^+, and its pH was adjusted to 10 before the experiment. It can be observed that the Li^+ adsorption capacity by the bilayer solar crystallizer is increased from 63.7-229.1 mg m^{-2} with the Li concentration increasing from 10–10000 μg L^{-1} (Figure S8), and the ratio of Li^+/Na^+ is also increased due to the higher adsorption amount. In contrast, the ratio of Li^+/Na^+ is lower than 10% in the single-layer solar crystallizer, even though the adsorption quantity is also increased from 12.5-109.7 mg m^{-2} with the Li^+ concentration increased (Figure 5e). That means the bi-layer structured solar structure is beneficial to the selectivity for Li adsorption. Compared to the bulk solution adsorption, the LTO loading on the non-woven fabric has a much higher exposure probability to the Li^+ due to the continuous brine flow on the non-woven fabric. Notably, the enthalpy change of the LTO chemical adsorption is positive (68.741 kJ mol^{-1}), thus, the high temperature during the solar-based crystallizer is beneficial for the Li^+ adsorption. Meanwhile, the concentration of Li^+ and Na^+ on the surface of the non-woven fabric will increase with water evaporation, and the Na^+ will rapidly reach saturation while the concentration of Li^+ is far from saturation. Therefore, both the concentration of Li^+ and the ratio of Li^+/Na^+ will be increased, which is beneficial for the adsorption of Li^+ by the LTO. This is the main mechanism for the advanced Li^+ adsorption capacity compared to bulk adsorption. Furthermore, the bilayer structure solar crystallizer separated the NaCl crystallization from the minor Li^+ ions' adsorption in the different layers, which is convenient for reducing the Na+ concentration in the inner layer to promote selective Li adsorption. Moreover, the selectivity of the divalent ions, particularly Mg^{2+}, with the Li^+ is important for the lithium extraction in the actual

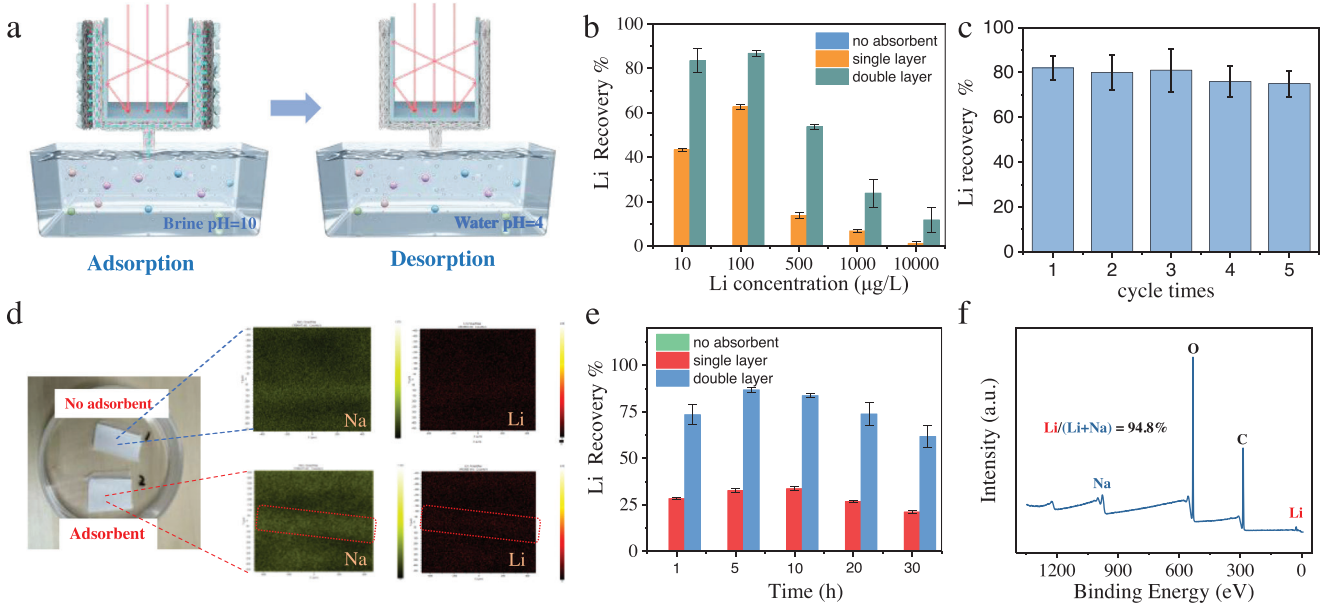

Figure 6. The schematic diagram for the recovery of the Li^+ in the solar-based system a); The Li recovery efficiency in different solar-based systems under different Li concentrations b); The cycling performance for the Li recovery efficiency of the bilayer solar-based crystallizer under 100 μg L^{-1} Li^+ concentration c); The Li and Na element XPS mapping of the inner layer for the bilayer solar-based crystallizer after the acid solution evaporation d); The Li recovery efficiency in the actual seawater e) and the surface element analysis of the ppy-fabric after the desorption f).

brine, thus, the Li^+ extraction in the mixed brine was conducted. It is shown in Figure 5f that the Li^+ concentration in the inner layer of the solar-based crystallizer is 18.5 to 47.8 times that of the Mg^{2+} and Ca^{2+}, indicating that the chemical adsorption of the LTO has high selectivity for the Li^+. Meanwhile, the bilayer structure of this solar crystallizer separated the crystallization of the Na^+, Mg^{2+}, and Ca^{2+} in the outer surface of ppy-fabric with the Li^+ adsorption in the inner space of the nonwoven fabric, which is also attributed to the high selectivity for the Li^+ extraction.

2.5. Selective Ion Recovery by the Bilayer Solar Crystallizer

The LTO can desorb the Li^+ under the acid condition, thus, this solar-based crystallizer can directly recover the LiCl by the evaporation of the acid water (**Figure 6a**). After the adsorption, the acid water (pH = 4) was used to replace the brine for the desorption and recovery of the LiCl, and the outer layer of the ppy-fabric was removed to reduce the influence of any residual NaCl in the ppy-fabric for the enhancement of the Li salt purity. It can be directly demonstrated that the loading of the LTO greatly promoted Li^+ recovery, which is 1–3 orders of magnitude higher than that of the nonwoven fabric without LTO (Figure 6b). Furthermore, the Li^+ recovery efficiency of the bilayer structure is 4–11.5 times that of a single-layer solar-based crystallizer (Figure 6b), probably due to the separation of the salt crystallization (NaCl) with the ions adsorption in the bilayer is helpful for the high-purity ions recovery. Before the desorption process, the outer layer of the ppy-fabric was removed to decrease the NaCl influence, thus the bi-layer structure solar crystallizer will increase the purity and the desorption efficiency of the Li ions. Meanwhile, the Li recovery proportion gradually decreased with the rise of the Li^+ concentration in the brine. This implies that the adsorption-based ions recovery technology is more suitable for recovering the low concentrations of ions in the brine. Meanwhile, this system can be cycled with the change of the bulk solution of brine and acid solution for the ions recovery, and the ions recovery efficiency is maintained during the five times cycle (Figure 6c). Meanwhile, the textile is corrosion-resistant to acid, alkaline, or seawater, thus it will be stable during the adsorption-desorption cycle. These results demonstrate that the LTO on the nonwoven fabric can directly adsorb the Li during the brine wicking and evaporation process, and the increase of the Li/Na ratio with the water evaporation is helpful for its recovery. After the desorption, X-ray photoelectron spectroscopy (XPS) was conducted for the Li and Na element mapping on the nonwoven fabric with or without LTO to directly demonstrate the adsorption of Li by the LTO on the nonwoven fabric. The results show the uniform distribution of the Li element on the fiber profile (Figure 6d), while it has a mixed and weak single peak for the Li element on the nonwoven fabric without adsorbent.

Moreover, the actual seawater was used for the demonstration of Li^+ recovery by this bilayer solar crystallizer. As shown in Figure 6e, 68% Li^+ can be recovered by this bilayer solar crystallizer through the adsorption-desorption cycle, which is 3–15 times that of the single-layer structure and 18–59 times that without the adsorbent, respectively. Furthermore, the salt component of the inner space of the bi-layer solar crystallizer ppy-fabric surface after the desorption process was analyzed by XPS (Figure 6f), and it directly proved that the high-purity LiCl (94.8%) can be crystallized in this bilayer solar crystallizer.

3. Discussion

3.1. DALT Fabric Promoted Stable Solar Evaporation

In this work, a unique salt crystallization behavior of the DALT fabric is discovered and investigated, that is, the salt with a loose structure is preferred to be crystallized on the surface of the fabric. The wetting gradient in the inner space of the DALT fabric is the main reason for this crystallization behavior. In the brine evaporation process, the wetting gradient in the DALT fabric ensures the fast liquid flow from the bulk solution to the evaporation interface, thus the nucleation process of salt ions is inhibited in the inner of the DALT fabric. Meanwhile, this fast liquid flow compresses the crystal growth space and shortens the crystal growth time (Figure 3d), thus it will have a small crystal size with a porous structure on the surface of the DALT fabric (Figure 3e,f). This salt crystallization behavior is beneficial to solve the scaling problem during the desalination process, which is further applied and demonstrated in the bilayer solar crystallizer. Nevertheless, all surfaces of the DALT fabric in this work are hydrophilic, while the salt crystallization has some abnormal phenomena on the hydrophilic surface. In our future work, the salt crystallization behavior in the DALT fabric with a hydrophobic interface, such as skin-like fabric, will be further investigated.

3.2. Bilayer Structure Solar Crystallizer for the Ions' Recovery

Recently, some work[5,28–32] also integrated the ion recovery system into the solar evaporation system (Table S2). For example, Han et al. constructed a photothermal fabric adsorbent for lithium extraction by encapsulating graphite powder and lithium-ion sieves with polyvinyl alcohol (PVA),[33] which is then simultaneously coated onto commercial cotton fabric. This system can remove 55% Li^+ from the solution after 0.5 h of adsorption. Chen et al. developed a high-performance solar-driven, direct lithium-extraction felt (DEF) for Li extraction in seawater and achieved 12 mg g^{-1} adsorption capacity under 1 sun irradiation.[34] The consensus from these works is that the high temperature from the photothermal conversion facilitates the Li adsorption, and the brine flow driven by the solar evaporation provides continuous and sufficient contact of the Li ions with the adsorbent. However, the scaling problem caused by the bivalent ions in the brine will hinder the brine evaporation and ions recovery efficiency, and the unique crystallization behavior of the DALT fabric is an effective solution for this problem. More importantly, the adsorption of the Li ions and other ions (Na^+, K^+, Ca^{2+}, Mg^{2+}) crystallization in the same fabric or system will impair the purity of recovered Li, and multiple steps are needed for the following Li salt recovery. In contrast, the separation of the Li adsorption and salt crystallization in the different layers (nonwoven fabric and ppy-fabric) will significantly reduce the concentration of non-target ions in the inner layer of the fabric for the high-purity Li extraction.

In general, the desalination of brine and recovery of low-concentration ions with high value can be simultaneously realized in this bilayer solar crystallizer. This bilayer structure of the solar-based crystallizer separated the brine-wicking channel with a salt crystallization interface, and most salt is crystallized on the surface of the DALT fabric with a loose structure rather than on the inner side, thereby promoting the long-term stable evaporation of the solar-based crystallizer. More importantly, the water evaporation in this bilayer solar crystallizer increases the concentration of trace ions (Li^+) as well as the relative ratio to the major ions, cooperating with the heat from the photothermal conversion to facilitate Li^+ adsorption and recovery. All these advantages of the bilayer solar crystallizer make it superior in terms of recovery efficiency compared to bulk solution adsorption. Moreover, the different layers for the adsorption and crystallization make the minor ions adsorption (Li^+) and the major ions (Na^+) crystallization completely separated in space, thus improving the recovery efficiency and the purity of high-value ions.

4. Conclusion

In this study, we discovered and systematically analyzed the unique brine transport and salt crystallization behavior within DALT fabric. Our findings reveal that the internal wetting gradient of DALT encourages porous salt to crystallize predominantly on its surface rather than within its inner layers. This phenomenon mitigates the blockage of wicking channels typically caused by salt crystallization. Leveraging this insight, we integrated DALT fabric into a solar crystallizer to develop a bilayer solar crystallizer for simultaneous brine evaporation with ion recovery. This bilayer solar crystallizer facilitates stable evaporation and crystallization of brine by effectively separating the crystallization surface from the wicking channel. Furthermore, by incorporating lithium adsorbent (LTO) into the inner layer of the bilayer solar crystallizer, we demonstrated efficient recovery of valuable Li^+ from seawater or brine during the desalination process, promising substantial economic benefits for brine treatment. Our results not only expand the application scope of DALT materials but also offer new insights into the fields of water-wicking materials and resource recovery within photothermal systems.

Supporting Information

Supporting Information is available from the Wiley Online Library or from the author.

Acknowledgements

This work was supported by the PolyU Academy for Interdisciplinary Research (PAIR) Young Fellowship for RAPs (Grant No. P0052939).

Conflict of Interest

The authors declare no conflict of interest.

Data Availability Statement

The data that support the findings of this study are available from the corresponding author upon reasonable request.

Keywords

brine treatment, directional liquid transportation, Li recovery, salt crystallization, solar evaporation

Received: May 7, 2025
Revised: June 25, 2025
Published online: August 13, 2025

[1] X. D. Zhang, Y. Q. Yao, T. Horseman, R. Y. Wang, Y. M. Yin, S. Z. Zhang, T. Z. Tong, S. H. Lin, *Nature Water* **2023**, *1*, 547.
[2] F. S. Pinto, R. C. Marques, *Renewable&Sustainable Energy Reviews* **2017**, *78*, 904.
[3] W. Zhao, H. Gong, Y. Song, B. Li, N. Xu, X. Z. Min, G. L. Liu, B. Zhu, L. Zhou, X. X. Zhang, J. Zhu, *Adv. Funct. Mater.* **2021**, *31*, 2100025.
[4] M. G. O'Connell, N. Rajendran, M. Elimelech, J. Gilron, J. B. Dunn, *Nature Water* **2024**, *2*, 1116.
[5] S. X. Yang, Y. G. Wang, H. Pan, P. He, H. S. Zhou, *Nature* **2024**, *636*, 309.
[6] L. F. Greenlee, D. F. Lawler, B. D. Freeman, B. Marrot, P. Moulin, *Water Res.* **2009**, *43*, 2317.
[7] R. Y. Wang, R. R. He, T. He, M. Elimelech, S. H. Lin, *Nature Water* **2023**, *1*, 291.
[8] N. Xu, J. L. Li, C. Finnerty, Y. Song, L. Zhou, B. Zhu, P. Wang, B. X. Mi, J. Zhu, *Nature Water* **2023**, *1*, 494.
[9] P. Tao, G. Ni, C. Y. Song, W. Shang, J. B. Wu, J. Zhu, G. Chen, T. Deng, *Nat. Energy* **2018**, *3*, 1031.
[10] W. B. Wang, Y. Shi, C. L. Zhang, S. Hong, L. Shi, J. Chang, R. Y. Li, Y. Jin, C. Ong, S. F. Zhuo, P. Wang, *Nat. Commun.* **2019**, *10*, 3012.
[11] A. F. Eskafi, C. De Finnda, C. A. Garcia, B. X. Mi, *Environ. Sci. Technol.* **2025**, *59*, 892.
[12] Y. J. Zheng, R. A. C. Gonzalez, K. B. Hatzell, M. C. Hatzell, *Joule* **2021**, *5*, 1971.
[13] Y. Shi, R. Y. Li, Y. Jin, S. F. Zhuo, L. Shi, J. Chang, S. Hong, K. C. Ng, P. Wang, *Joule* **2018**, *2*, 1171.
[14] C. Wang, H. C. Zhang, Z. X. Kang, J. T. Fan, *Adv. Sci.* **2024**, *11*, 2305313.
[15] C. L. Zhang, Y. Shi, L. Shi, H. X. Li, R. Y. Li, S. Hong, S. F. Zhuo, T. J. Zhang, P. Wang, *Nat. Commun.* **2021**, *12*, 998.
[16] H. W. Chen, P. F. Zhang, L. W. Zhang, H. L. L. Iu, Y. Jiang, D. Y. Zhang, Z. W. Han, L. Jiang, *Nature* **2016**, *532*, 85.
[17] K. C. Park, P. Kim, A. Grinthal, N. He, D. Fox, J. C. Weaver, J. Aizenberg, *Nature* **2016**, *531*, 78.
[18] C. C. Liu, J. Ju, J. Ma, Y. M. Zheng, L. Jiang, *Adv. Mater.* **2014**, *26*, 6086.
[19] X. M. Dai, N. Sun, S. O. Nielsen, B. B. Stogin, J. Wang, S. K. Yang, T. S. Wong, *Sci. Adv.* **2018**, *4*, aaq0919.
[20] M. J. Qazi, H. Salim, C. A. W. Doorman, E. Jambon-Puillet, N. Shahidzadeh, *Sci. Adv.* **2019**, *5*, aax1853.
[21] H. C. Zhang, Z. X. Kang, Y. X. Wu, Y. Pu, S. K. Jiang, S. Amir, P. Wang, J. T. Fan, *Nano Energy* **2024**, *128*, 109919.
[22] T. De Kock, M. A. Boone, T. De Schryver, J. Van Stappen, H. Derluyn, B. Masschaele, G. De Schutter, V. Cnudde, *Environ. Sci. Technol.* **2015**, *49*, 2867.
[23] K. Chen, L. X. Li, B. C. Li, Y. F. Yang, K. Y. Zhu, J. P. Zhang, *Adv. Funct. Mater.* **2024**, *34*, 2402221.
[24] R. J. Ding, J. H. Xiong, Q. Yan, P. Y. Li, X. Zhao, Z. Chen, Z. L. Liu, H. X. Lian, Z. G. Tang, S. Y. Du, Q. Y. Peng, X. D. He, *Chem. Eng. J.* **2024**, *481*, 148364.
[25] R. J. Ding, H. W. Zheng, X. Zhao, F. H. Xue, P. Y. Li, J. H. Xiong, Z. Chen, Z. L. Liu, Q. Y. Peng, X. D. He, *Applied Science and Manufacturing* **2022**, *158*, 106967.
[26] S. X. Zheng, B. Oelckers, A. Khandelwal, Z. J. Ren, *Nature Water* **2025**, *3*, 135.
[27] X. C. Sun, P. V. Radovanovic, B. Cui, *New J. Chem.* **2015**, *39*, 38.
[28] Q. H. Liu, Z. Yu, Y. X. Zhang, K. Mao, W. E. Xiang, S. Guo, T. Xiong, S. C. Tan, *Chem. Eng. J.* **2025**, *506*, 159990.
[29] Y. Song, S. Q. Fang, N. Xu, M. N. Wang, S. Y. Chen, J. Chen, B. X. Mi, J. Zhu, *Science* **2024**, *385*, 1444.
[30] Z. W. Qiu, M. Y. Wang, Y. Chen, T. Zhang, D. Y. Yang, F. X. Qiu, *Desalination* **2021**, *506*, 115003.
[31] Z. X. Meng, M. L. Wang, X. Cao, T. Wang, Y. C. Wang, Y. K. Xu, W. F. Liu, L. Chen, Y. Z. Huang, X. G. Liu, *Chem. Eng. J.* **2022**, *445*, 136780.
[32] L. Tang, S. D. Huang, Y. Wang, D. X. Liang, Y. D. Li, J. Li, Y. G. Wang, Y. J. Xie, W. Wang, *ACS Appl. Mater. Interfaces* **2020**, *12*, 9775.
[33] Z. H. Han, S. M. Qi, M. T. Fu, L. Han, C. X. Hong, Z. Y. Shen, X. C. Wang, K. Y. Su, X. G. Xue, B. W. Zhang, J. Z. Gu, H. J. Ma, *Adv. Funct. Mater.* **2025**, *35*, 2422901.
[34] X. Chen, W. H. Yu, Y. Zhang, C. Huang, L. Nie, J. M. Yu, Y. Y. Zhang, C. Zhang, W. B. Zhai, X. S. Zhang, Y. Yu, W. Liu, *Adv. Funct. Mater.* **2024**, *34*, 2316178.